



High-Resolution Simulations: Modeling Intracluster Medium and Dark Matter in Galaxy Cluster

Elena Rasia^{1,*} Giuseppe Tormen¹
and Lauro Moscardini²

¹ Dipartimento di Astronomia, Università di Padova, vicolo dell'osservatorio 2,
35122 Padova, Italy

² Dipartimento di Astronomia, Università di Bologna, via Ranzani 1, 40127
Bologna, Italy

Abstract. Using high-resolution simulations of galaxy clusters we provide new models in a simple analytic form to describe the average radial profiles of the main quantities of the baryonic and dark matter components. With these models we construct a self-consistent dynamical model which can be used to estimate the cluster masses.

Key words. cosmology: theory – galaxies: clusters – X-rays: galaxies – dark matter – methods: numerical

1. Introduction

Galaxy clusters are the largest gravitationally bound systems in the universe and they are ideal objects for cosmological studies. In fact they represent a tool to understand the structure formation at large scale and to constrain the different parameters describing the cosmological models.

To study from theoretical point of view these systems, the numerical approach is better than the analytical one. In fact this technique does not need simplifying approximations.

In our work we used 17 galaxy clusters simulated with high resolution. The parti-

cle number inside the virial radius is very high, of order of 10^5 . This implies very high resolution in mass and in force. For this reason we can resolve the inner part of the clusters and study the physical processes also at small scale.

The plan of the paper is as follows. In Section 2 we present our simulations. In Section 3 and 4 we describe the dark matter and gas profiles, respectively, and we derive and test different methods to estimate the cluster mass. Finally in Section 5 we summarize our results.

* Contact email address: rasia@pd.astro.it

2. Numerical Simulations

In order to obtain a large sample of simulated high-resolution clusters we use the technique of re-simulation called ZIC (Zoom Initial Condition), described in much more detail in Tormen (1997). Here we give only a brief summary of the adopted procedure. Much more details can be found in the original paper.

Using the results of a cosmological N-body simulation (i.e. with a box-size of approximately 500 Mpc/h and obtained considering only dark matter particles), in the output at $z = 0$ we identify the galaxy clusters using the method of spherical over-density. Then we recover in the initial conditions the (extended) Lagrangian region from where each cluster originated. Here we produce new initial conditions by increasing the number of the particles by a factor of $10^2 - 10^3$. On the contrary, outside this region the number of particles is strongly reduced by substituting all the particles in a fixed zone with a single particle positioned in the barycenter with a mass equal to the total mass particles. This method allows to have at the same time a very good resolution in the region where cluster forms and good representation of the external tidal forces.

Starting from the new initial conditions, a new simulation is evolved using the code GADGET (GALaxies with Dark matter and Gas intEract, Springel et al. 2001). This is a TREEsph code where the dark matter particles are evolved using a tree-code (Barnes & Hut) while the collisional gas is followed using the SPH (Smoothed Particle Hydrodynamics) approach.

At the end inside each cluster we have approximately a million of particles for both components. The mass of the dark matter and gas particles are around $m_{DM} = 2 - 5 \cdot 10^9 M_\odot/h$, and $m_{gas} = 2 - 5 \cdot 10^8 M_\odot/h$, respectively.

The cosmological model used is a flat Λ CDM, with $\Omega_M=0.27$, $\Omega_B=0.03$, $\Omega_\Lambda=0.7$, the Hubble parameter is $h = 0.7$

and the power-spectrum normalization corresponds to $\sigma_8 = 0.9$.

Our final sample includes 17 high-resolution clusters, with a mass ranging between $3.6 \cdot 10^{14} M_\odot/h$ and $1.5 \cdot 10^{15} M_\odot/h$ and with a virial radius between 1.5 Mpc/h and 2.5 Mpc/h.

3. Dark Matter Profiles

3.1. Density and velocity

First we estimate for each simulated cluster the profile of the dark matter component. Figure 1 shows the average profile (computed on the whole sample) with its error. The dotted line shows the NFW model (Navarro, Frenk & White 1995, 1996, 1997) which is largely used in the literature to describe the distribution of the dark matter component. Its expression is:

$$\rho(r) = \frac{\rho_0 x_s}{x(1+x/x_s)^2} \quad \text{where} \quad (1)$$

$$\rho_0 = \frac{\Delta_v}{3x_s^3[\ln(1+1/x_s) - 1/(1+x_s)]}. \quad (2)$$

Integrating the previous relation, it is possible to obtain the mass as:

$$M_{NFW}(x) = \left[x \frac{(\ln(1+cx) - (cx)/(1+cx))}{(\ln(1+c) - c/(1+c))} \right]^{0.5} \quad (3)$$

and the potential:

$$\Phi_{NFW}(x) = -4\pi G \rho_0 \frac{x_s^3}{x} \ln \left(\frac{x_s + x}{x_s} \right) \quad (4)$$

In these equations there are two parameters: the virial over-density, Δ_v , that depends on the cosmological model and on the contribution of dark matter mass to the total mass, and the concentration parameter c , which is related to the scale parameter x_s as $c = 1/x_s$.

Figure 1 shows that for distances $0.05 < r/r_v < 0.3$ the NFW model does not give a good fit of the dark matter density profiles of our simulated clusters.

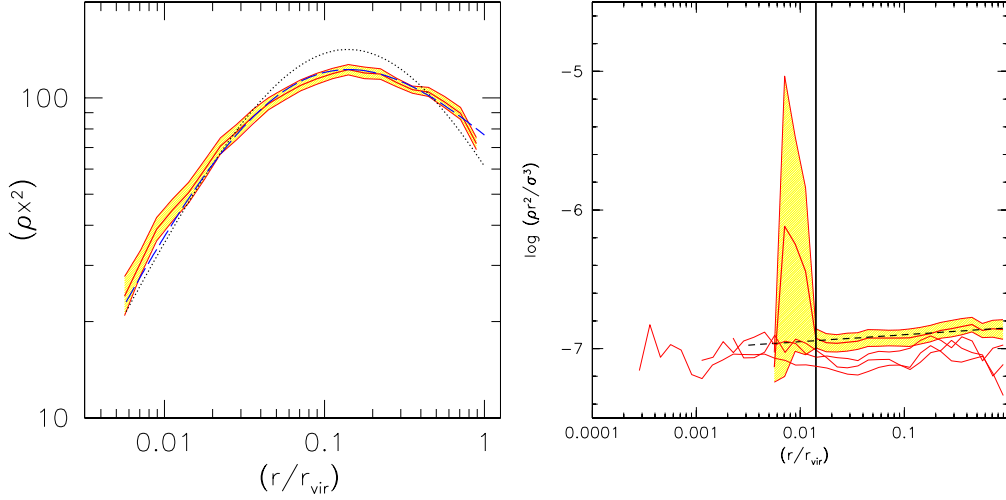


Fig. 1. Left panel: the dark matter radial profile of ρx^2 , the dotted line is the NFW model (equation 1); right panel: the dark matter radial profile of $\rho x^2/\sigma^3$ (phase space density profile times x^2); the three solid lines are the profiles of a cluster re-simulated with increasing resolution (the particles number inside the virial radius is respectively $6 \cdot 10^5$, $3.4 \cdot 10^6$ and $1.9 \cdot 10^7$). In both plots: the shaded zone represents the error related to the average, the solid line inside this zone is the average radial profile and the dashed line is our model.

In order to improve the fit also in this range, we propose a different model which satisfies two conditions: 1) to have only one scale parameter and 2) to have a simple analytic form, with a double power-law.

To build our model, we first notice that the phase-space density profiles can be fitted using a simple power-law relation:

$$\rho/\sigma^3 \propto r^\alpha, \quad (5)$$

with $\alpha = -1.95$ (see the right panel of Fig. fig:rhodm). For $r < 0.01$ the average profile shows a large fluctuation, which is due to numerical effects. In fact this irregular behavior is not shown by the profiles of clusters simulated with higher resolution (represented by solid lines in the same figure).

Now we need to consider the velocity profiles, which are important not only to understand the dark matter distribution in the cluster, but also to estimate the total mass through the Jeans equation. For this purpose the simplest approach is to assume that the velocity field is isotropic, but on

average this condition is not satisfied, so a different more realistic model is required.

Here we present the profiles for:

1. the radial velocity dispersion σ_r/σ_v ;
2. the tangential velocity dispersion σ_t/σ_v ;
3. the radial velocity v_r/σ_v ;
4. the velocity anisotropy parameter $\beta = 1 - \sigma_t^2/2\sigma_r^2$.

The first three quantities have been normalized by the virial radial dispersion σ_v derived from the Virial Theorem: $\sigma_v^2/r_v \approx GM_v/r_v^2$. The β parameter gives information on the velocity field: $\beta = 0$ means that there are isotropic motions, $\beta < 0$ and $\beta = 1$ mean that there are only tangential and radial motions, respectively.

The results are shown in Figs. fig:sigdm and fig:veldm. The behaviors of the velocity dispersion and anisotropy parameter confirm that in general clusters are not isothermal. Instead, the trend of β suggests the predominance of radial motions near the

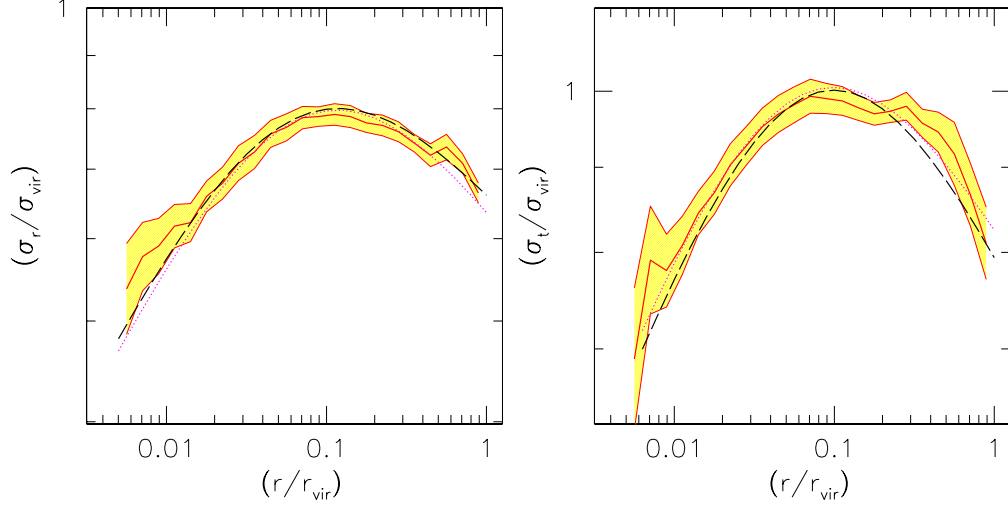


Fig. 2. Left panel: The dark matter radial velocity dispersion profile. Right panel: The dark matter tangential velocity dispersion profile. See legend to figure 1 for description of the lines and other details of the plot.

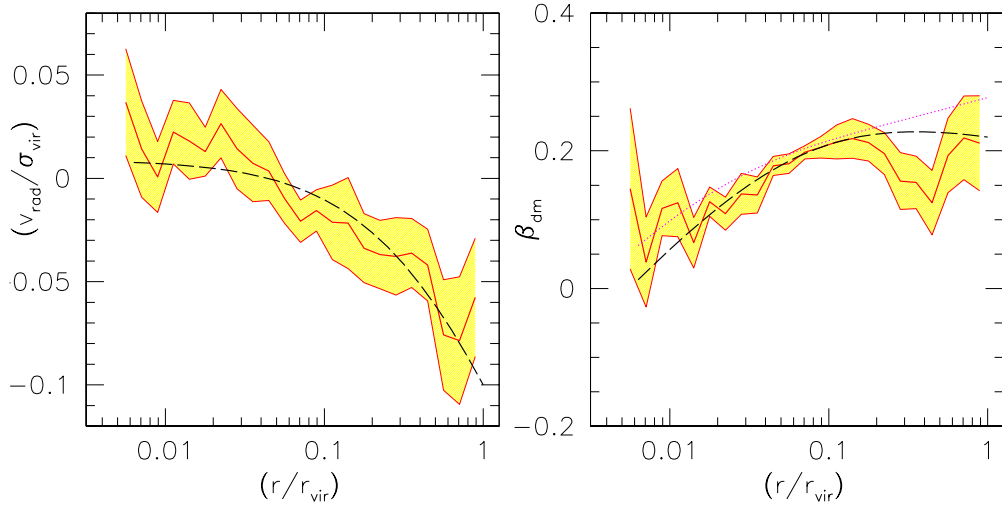


Fig. 3. Left panel: The dark matter radial velocity profile. Right panel: The dark matter anisotropy velocity dispersion profile. See legend to figure 1 for description of the lines and other details of the plot

virial radius, while in the inner zone there is a more isotropic field.

We decided to fit the velocity profiles using relations satisfying the same conditions applied for density. We obtain the following expressions:

1. for the average radial velocity dispersion profile, σ_r/σ_v :

$$\tilde{\sigma}_r(x) = Nx^{0.3}(x+x_p)^{-0.48},$$

$$\text{where } x_p = 10^{-1.15}, N = 0.68; \quad (6)$$

2. for the average tangential velocity dispersion profile, σ_t/σ_v :

$$\tilde{\sigma}_t(x) = Nx^{0.25}(x+x_p)^{-0.45},$$

$$\text{where } x_p = 10^{-1.1}, N = 0.82; \quad (7)$$

3. for the average radial velocity profile, v_r/σ_v :

$$\tilde{v}_r(x) = v_r(x)/\sigma_v = N(x+x_p)^{-0.2}, \quad (8)$$

$$\text{where } x_p = 10^{-0.4}, N = 0.85;$$

4. for the average anisotropy parameter profile, β :

$$\tilde{\beta}(x) = Nx^{0.25}(x+x_p)^{-0.3}, \quad (9)$$

$$\text{where } x_p = 10^{-1.15}, N = 1.69.$$

Combining the phase-space density profile with the radial velocity dispersion profile, we can now obtain our model for the density in the ordinary space:

$$\rho(r) = \frac{\rho_0}{x(x+x_p)^{1.5}} \quad \text{where} \quad (10)$$

$$\rho_0 = \frac{\Delta_v}{6 \left[(1+2x_p)/(1+x_p)^{0.5} - 2x_p^{0.5} \right]};$$

$$x = r/r_v. \quad (11)$$

This fit, shown by the dashed line in the left panel of Fig. fig:rhodm describes the simulated data more properly than the NFW model in the inner part of the cluster (for $r < 0.7r_v$).

We can compute from our model the mass as:

$$\frac{\tilde{M}}{M_v}(x) = \frac{6\rho_0}{\Delta_v} \left[\frac{x+2x_p}{(x+x_p)^{0.5}} - 2x_p^{0.5} \right] \quad (12)$$

and the potential:

$$\tilde{\Phi}(x) = -16\pi r_v^2 \rho_0 \left[\frac{x_p}{\sqrt{x^2(x+x_p)}} - x_p^{0.5} \right]. \quad (13)$$

3.2. Mass Estimates

The mass for a collisionless system can be derived through the Jeans equation. Studying this equation we can test the equilibrium of the dark matter and the self-consistency of our density and velocity models.

For a spherical, steady system the Jeans equation can be expressed by:

$$\frac{M^J}{M_v}(x) = \quad (14)$$

$$-x \frac{\sigma_r^2}{\sigma_v^2} \left[\frac{d \ln \rho}{d \ln r} + \frac{d \ln \sigma_r}{d \ln r} + 2\beta \right].$$

In Fig. 4 we show the comparisons between the true mass profile, i.e. the average mass profile of our simulated clusters, and the analytic mass, as derived by the Jeans equation (including the NFW density profile, curve labeled 3, and our profile, curve 2) or by the integrals of the density models: M_{NFW} (eq. 3 and curve 1) and \tilde{M} (eq. 12 and curve 4).

We notice that our model agrees with the simulations much better than the NFW one. Moreover for $r > 0.02r_v$ the Jeans equation properly estimates the total mass with an error $< 10\%$ both for NFW and our fits.

4. Gas Profiles

4.1. Density and velocity

The β -model (Cavaliere & Fusco-Femiano 1976, 1978), generally used to fit the observed gas density profile, is not able to reproduce the central and external parts of the cluster profile. Moreover it does not agree with simulations (Navarro, Frenk & White 1995; Bartelmann & Steinmetz 1996).

In Fig. 5 we compare the gas and the dark matter density profile and we can notice two important results. First, the gas profile is smoother in the internal region, this is due to the gas high pressure that balances the gravitational force in the central

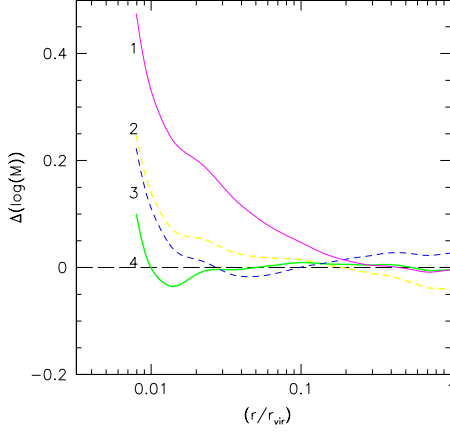


Fig. 4. Comparison between the true mass and M_{NFW} (line 1); \tilde{M}^J (line 2); M_{NFW}^J (line 3); \tilde{M} (line 4).

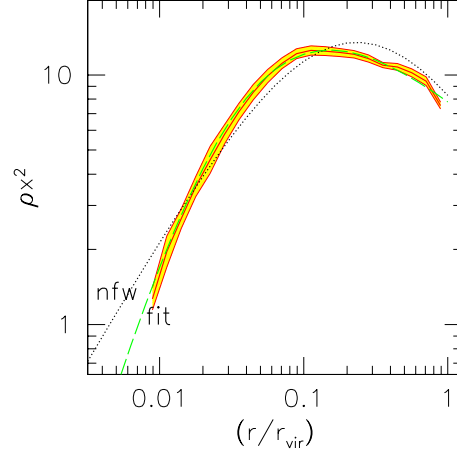


Fig. 6. The average gas density profile. The dotted line is the best fit of a NFW model. See legend to figure 1 for description of the lines and other details of the plot.

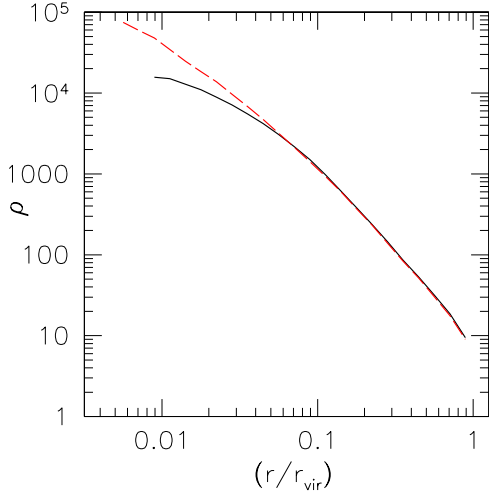


Fig. 5. Dark matter (dashed line) and gas (solid line) density profiles, normalized in order to reach the same value at the virial radius.

zone. Second, the profiles are self-similar for $r > 0.06r_v$.

We decide to fit the gas density profile with a double power-law, where the asymptotic behaviors are fixed and the scale radius is chosen “ad hoc”.

In Fig. (6) we show our results for the average density profile times radius squared, $\log(\rho x^2)$. In the plot the dashed line represents our model which is built with the same characteristics of the dark matter model.

The analytic expression of our model is:

$$\tilde{\rho}(x) = \frac{\rho_0}{(x + x_p)^{2.5}} \quad \text{where} \quad (15)$$

$$x = r/r_v; \quad x_p = 0.04 r_v;$$

$$\rho_0 = \quad (16)$$

$$3 \left[\frac{\Delta_v}{\left[\frac{16/3x_p^3 + 40/3x_p^2 + 10x_p + 2}{(x_p + 1)^{2.5}} - 16/3x_p^{0.5} \right]} \right].$$

Our model asymptotically tends to a constant value in the limit $r \rightarrow 0$ and decreases in the outer part with an asymptotic law similar to the dark matter one, $\rho \propto r^{-2.5}$.

As for the dark matter profiles, the dispersions and the radial velocity are normalized dividing by the virial velocity dispersion σ_v . The anisotropy parameter profile is not the average, but the median profile.

The velocity behaviors are very different for the two components (compare Figs. (2 and 3 to Figs. 7 and 8). This difference occurs because the forces acting on the gas and on dark matter are not the same. The radial velocity decreases near the virial radius, while in the center is almost constant and/or negative, suggesting that the gas is still infalling.

In Figs. 7 and 8 the dashed lines refer to our models:

$$\tilde{\sigma}_r(x) = \sigma_r/\sigma_v = \frac{N}{(x_p + x)^{0.5}} \quad (17)$$

where $N = 0.46$, $x_p = 10^{-1.72}$;

$$\tilde{\sigma}_t(x) = \sigma_t/\sigma_v = \frac{Nx^{0.6}}{(x_p + x)^{0.5}} \quad (18)$$

where $N = 0.54$, $x_p = 10^{-1.1}$;

$$\tilde{\beta}(x) = 1 - \frac{\tilde{\sigma}_t}{2\tilde{\sigma}_r}, \quad (19)$$

where $\tilde{\sigma}_r$ and $\tilde{\sigma}_t$ are described in eqs.(4.1)and (4.1).

4.2. Temperature

In Fig. 9 we show the average temperature profile normalized to the value, T_0 :

$$T_0 = 1.35 \left(\frac{G\mu m_p M_v}{k_b r_v} \right), \quad (20)$$

where G is the gravity constant, μ the medium molecular weight (we assume $\mu = 0.59$ for the ICM), m_p the proton mass and k_b the Boltzmann constant.

The inner region is nearly isothermal up to $r \approx 0.2r_v$, showing only a very small positive gradient. At larger radii the temperature decreases, assuming at the virial radius a value which is almost half of the central value. The profile we found agrees with previous numerical works (Navarro et al. 1995; Eke et al. 1998; Bryan & Norman 1998; Frenk et al. 1999; Thomas et al. 2001) and also with the temperature profile found from the analysis of the Beppo-SAX data

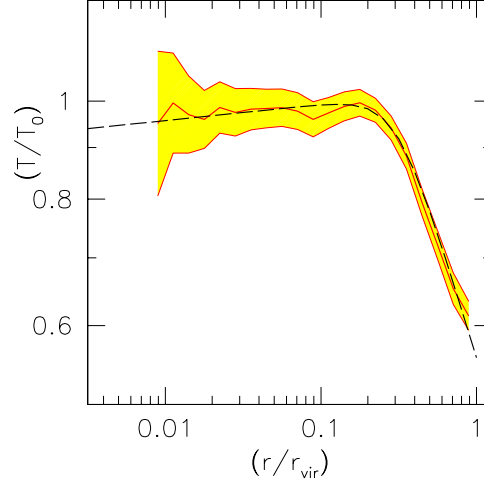


Fig. 9. The temperature profile. See legend to figure 1 for description of the lines and other details of the plot.

by De Grandi & Molendi (2002). Our data are well described by the relation:

$$\tilde{T} = T/T_0 = \frac{x^{0.016}}{(1 + x^4/x_T)^{0.13}}, \quad (21)$$

where $x = r/r_v$; $x_T = 0.009$ and T_0 , as in eq. (20).

4.3. Mass Estimates

Usually the hydrostatic equilibrium is assumed to derive a mass estimate from X-ray data. High-resolution simulations can give some indications on the accuracy of this assumption.

Assuming that the gravitational potential is static and spherical, and that the velocity field is isotropic ($\beta \equiv 0$) and substituting the dark matter velocity dispersion (σ_{rDM}) with the virial temperature, through the expression:

$$k_b T / \mu m_p = \sigma_{rDM}^2, \quad (22)$$

we obtain the hydrostatic equilibrium equation:

$$M(< r) = -\frac{r k_b T(r)}{G \mu m_p} \left[\frac{d \ln \rho}{d \ln r} + \frac{d \ln T}{d \ln r} \right]. \quad (23)$$

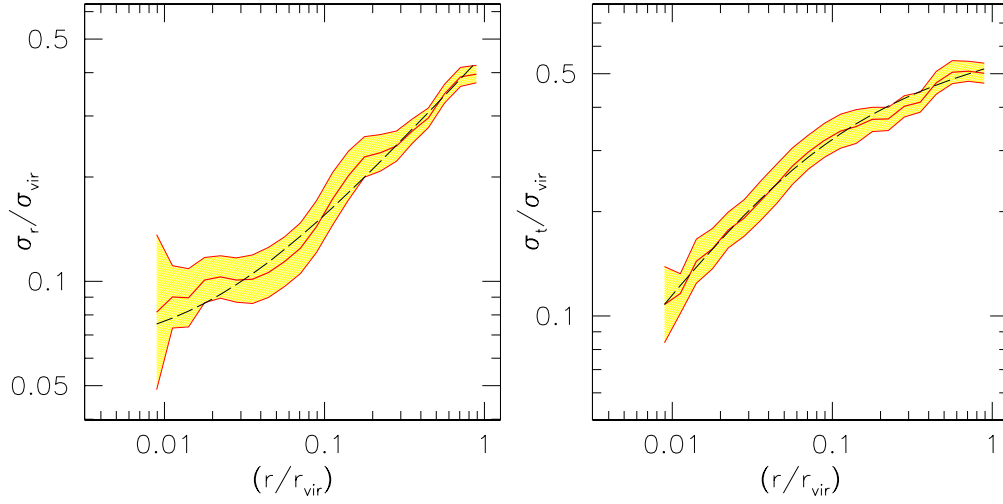


Fig. 7. Left panel: the gas radial velocity dispersion profile. Right panel: the gas tangential velocity dispersion profile. See legend to figure 1 for description of the lines and other details of the plot.

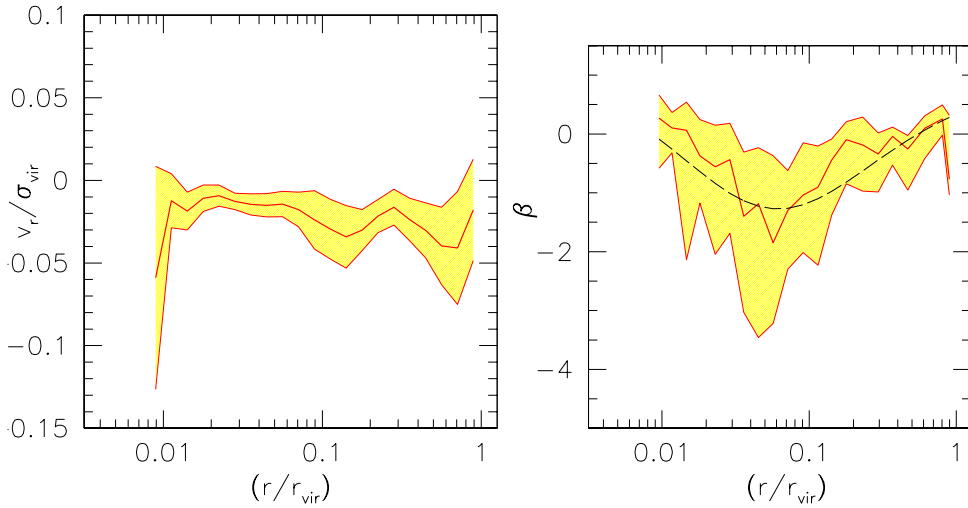


Fig. 8. Left panel: The gas radial velocity profile. Right panel: The gas anisotropy velocity dispersion profile. See legend to figure 1 for description of the lines and other details of the plot.

The hypothesis done to obtain this equation are too much restrictive for three different reasons. First, the β parameter is not always zero (see Fig. 8). Second, the substitution of the velocity dispersion with the temperature is not justified. Third, the

gas velocity dispersion is not considered in this derivation.

From the equation describing a system in a spherical and symmetrical potential:

$$\frac{d\Phi}{dr} = \frac{1}{\rho} \frac{dP}{dr} + \frac{1}{\rho} \frac{d(\rho\sigma_r^2)}{dr} + 2\frac{\beta\sigma_r^2}{r}, \quad (24)$$

where σ_r is the radial velocity dispersion, we substitute $P = \rho k_b T / \mu m_p$ and $\Phi = MG/r$ to obtain a new mass estimate:

$$\frac{M(< r)}{M_v} = -\frac{r}{GM_v} \frac{T(r)}{\mu m_p / k_b} \left[\frac{d \ln \rho(r)}{d \ln r} + \frac{d \ln T(r)}{d \ln r} \right] - \frac{r}{GM_v} \sigma_r^2(r) \left[\frac{d \ln \rho(r)}{d \ln r} + \frac{d \ln \sigma_r^2(r)}{d \ln r} + 2\beta(r) \right]. \quad (25)$$

To estimate the mass we use the following models:

1. isothermal sphere:

$$M_1^E(< x) = -x[\tilde{T} - 2] \quad (26)$$

where (-2) is the power-law $d \log \rho / d \log r$ of this model;

2. hydrostatic equilibrium, described by eq. (23):

$$M_2^E(< x) = -x\tilde{T} \left[\frac{d \ln \tilde{\rho}}{d \ln x} + \frac{d \ln \tilde{T}}{d \ln x} \right] \quad (27)$$

3. the model described in eq. (25):

$$M_3^E(< x) = -x\tilde{T} \left[\frac{d \ln \tilde{\rho}}{d \ln x} + \frac{d \ln \tilde{T}}{d \ln x} \right] + x\tilde{\sigma}_r^2 \left[\frac{d \ln \tilde{\rho}}{d \ln x} + \frac{d \ln \tilde{\sigma}_r^2}{d \ln x} + 2\tilde{\beta} \right] \quad (28)$$

where M^E is the mass normalized by the virial mass and $x = r/r_v$.

As shown in Fig. 10 the isothermal sphere does not agree at all with the true mass. In fact in the central region the discrepancies are of the order of a factor 10. The mass derived from the hydrostatic equilibrium describes quite properly the true mass for $r > 0.05r_v$, but tends to overestimate the inner mass. Finally, using the complete equation (including both the

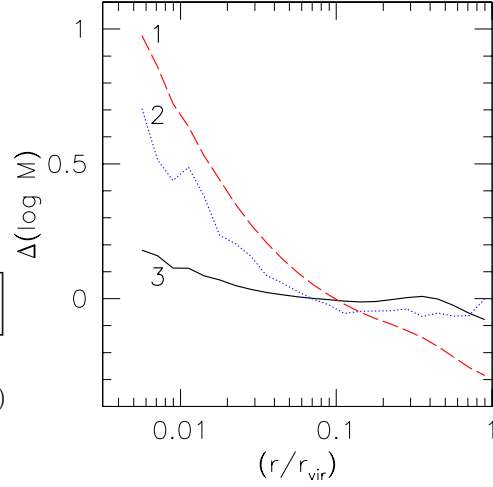


Fig. 10. Comparison between the true mass and M_1^E (line 1), M_2^E (line 2) M_3^E (line 3)

velocity dispersion and the anisotropy parameter) we obtain the best fit, in particular in the very central part, where it has a maximum error of 20%. Around the virial radius there is a slight difference with the true mass: this depends on the fact that our model for the radial velocity dispersion is not perfect in this region.

5. Conclusions

For the dark matter, we propose a model for the density profile which gives a more accurate description than the NFW model. Moreover we present new simple fits for velocity profiles which can be used to construct a self-consistent dynamical model, useful also for mass estimates. We find that the Jeans equation gives a realistic estimate of the mass (error < 10%).

For the gas distribution we find out an analytic fit for density, temperature and velocity dispersions. Since the gas is not really in hydrostatic equilibrium ($\sigma \neq 0$) and the velocity field is not isotropic, we include the terms related to σ_r and β in the equation of hydrostatic equilibrium to have better mass estimates.

The resulting models describe the average properties of galaxy clusters and have immediate applications for X-ray, SZ and lensing observations.

Acknowledgements. This work has been partially supported by Italian MIUR (Grant 2001, prot. 2001028932, “Clusters and groups of galaxies: the interplay of dark and baryonic matter”), CNR and ASI.

References

- Bartelmann, M., & Steinmetz, M., 1996, MNRAS, 283, 431B
- Bryan, G., & Norman, M. L., 1998, ApJ, 495, 80B
- Cavaliere, A., Fusco-Fermiano, R., 1976, A&A, 49, 137
- Cavaliere, A., Fusco-Fermiano, R., 1978, A&A, 30, 677
- De Grandi, S., & Molendi, S., 2002, ApJ, 567, 1
- Eke, V. R., Navarro, J. F., & Frenk, C.S., 1998, ApJ, 503, 569
- Frenk, C. S. et al. 1999, ApJ, 525, 554
- Navarro, J.F., Frenk, C. S., & White, S. D.M., 1995, MNRAS, 275, 720
- Navarro, J.F., Frenk, C. S., & White, S. D.M., 1996, ApJ, 462, 563
- Navarro, J.F., Frenk, C. S., & White, S. D.M., 1997, Apj, 490, 493
- Springel, V., Yoshida, N., & White, D. M., 2001, New Astronomy, 6, 79
- Thomas, P. A., et al. 2001, MNRAS, 324, 450T
- Tormen, G., 1997, MNRAS, 290, 411
- Tormen, G., Bouchet, F. R., & White, S. D. M., 1997, MNRAS, 286, 865